Physica Medica 65 (2019) 200–208

Contents lists available at ScienceDirect

Physica Medica

journal homepage: www.elsevier.com/locate/ejmp

Original paper

Sparse proportional re-scanning with hadron beams

Ugo Amaldi[a], Caterina Cuccagna[a,b,*], Alessandra Lo Moro[a,c], Valeria Rizzoglio[a,d], Jacques Bernier[e], Shelley Bulling[e]

[a] TERA Foundation, CERN, 1211 Geneva, Switzerland
[b] University of Geneva, 1205 Geneva, Switzerland
[c] Politecnico di Torino, 10129 Turin, Italy
[d] CERN, 1211 Geneva, Switzerland
[e] Clinique de Genolier, 1272 Genolier, Switzerland

ARTICLE INFO

Keywords:
Hadron therapy
Particle therapy
Proton dose delivery
Spot scanning
Re-scanning
Re-painting

ABSTRACT

Spot Scanning is a well-established technique to deliver the dose with hadron therapy systems. For many years re-scanning (called also re-painting) has been used to achieve uniform dose distribution in particular for moving organs, although it leads to an increase of the treatment time. Reducing this time is a major focus of present research. In this paper, after reviewing the current re-scanning techniques, *sparse proportional re-scanning* is defined and applied to 29 proton patient cases for a total of 54 fields. In this technique, only the highest weighted spot in the whole target is visited a number of times that is equal to the number N of re-scans. The number of visits of the beam spot to all remaining spots is scaled down proportionally to their weight. Sparse proportional re-scanning is advantageous especially in volumetric re-scanning. In order to quantify the potential advantages of this technique in terms of treatment time, *a reduction factor* of the number of scanned spots has been introduced, evaluated and analysed for 54 proton fields. The conclusion is that the reduction factor is a function of N (having values equal to 2.8 ± 0.3 and 3.6 ± 0.4 for $N = 5$ and $N = 12$ respectively) and does not depend either on the shape and volume of the target or on the distance between the scanned layers and the spot grid. The same values are approximately valid also for carbon ion treatments.

1. Introduction

For many years active raster scanning, used initially with synchrotrons beams [1], and Spot Scanning, introduced for cyclotron beams [2,3] have been recognized as very effective techniques for irradiating a tumour with beams of charged hadrons. With time these two techniques have converged even if, for historical reasons, many still use different names. In all instances the tumour target is irradiated by moving the "beam spot" of a charged hadron beam, which is due longitudinally to the Bragg peak and transversally to the beam transverse dimensions combined with the effect of multiple scattering in the traversed matter. Most often the beam is not switched off during a transverse movement. Longitudinally the spot depth (i.e. its energy) is varied with methods that depend on the accelerator type while transversally it is always moved acting on two "scanning magnets" placed some meters upstream of the patient, as shown in Fig. 1.

Cyclotrons produce fixed energy beams so that movable absorbers and collimators are used; the minimum time needed for an energy change is 100–200 ms, but often it is much larger. The protons and carbon ions beams extracted from synchrotrons have the energy required to reach the target layer to be irradiated and thus do not need absorbers of variable thickness. In a synchrotron, using the RF knock-out extraction technique, the minimum time needed to change energy is 100–200 ms [4]. The energy of the beams accelerated by hadron linacs can be varied pulse-by pulse so that for hadrons, which run with 200–400 Hz repetition rates, the energy changing time is about 5–2.5 ms, more than 20 times smaller than the ones of cyclotrons and synchrotrons [5].

The Treatment Planning System (TPS) outputs the space positions of the S "planned spots", which are usually placed, longitudinally, in L Equal-Energy Layers (each corresponding to a different beam energy) and, in each layer, on a transverse rectangular "spot grid" with spot spacing equal to Δ. During the dose delivery, when the beam spot has been moved to "visit" the next planned spot, the beam current is kept "on" till some monitors, in particular the ones that are placed upstream of the patient, register the number of protons (or ions) required by the TPS. In this paper, dose delivery procedures of this type are all called active "Spot Scanning" even if in many synchrotron centres are called

* Corresponding author.
E-mail addresses: ugo.amaldi@cern.ch (U. Amaldi), caterina.cuccagna@cern.ch (C. Cuccagna).

https://doi.org/10.1016/j.ejmp.2019.07.022
Received 5 February 2019; Received in revised form 30 June 2019; Accepted 26 July 2019

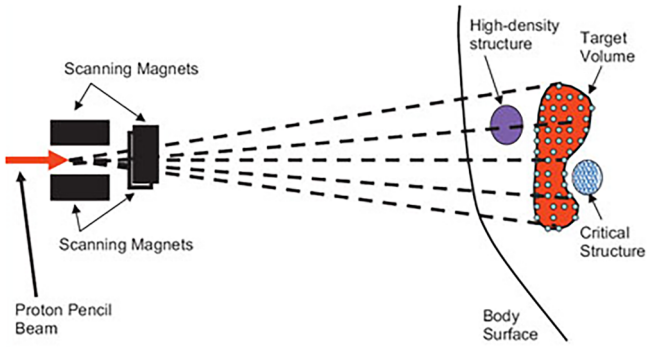

Fig. 1. Diagram of a typical active Spot Scanning technique. The blue dots are the centres of the planned spots. (Courtesy of the MD Anderson Cancer Centre.) (For interpretation of the references to colour in this figure legend, the reader is referred to the web version of this article.)

"Raster Scanning".

The potentiality and flexibility of the Spot Scanning method for treating different kinds and sizes of lesions is well known and already confirmed [6]. In spite of the confirmed success of this technique in treating static tumours, limitations appear in case of moving organs because the interplay between the scanning beam and the organ motion leads to a deterioration of the dose distribution and, potentially, a reduced tumour control [7].

A first method to mitigate the interplay effects consists in increasing the safety margins and expanding the clinical target volume. However, it has been demonstrated that this practice, in combination with Intensity Modulated Particle Therapy (IMPT) plans, may lead to inhomogeneous dose distributions [8].

Current research in accelerator developments and dose delivery techniques focuses on the use of the so-called "re-scanning" or "repainting" techniques. Introduced for the first time in 1992, the rescanning of the target volume several times averages out the interplay effects [9]. By combining this approach with gating, breath hold or "4D tracking" of the moving target the dose distribution can be made more conformal and uniform.

In the last years, several studies have been performed comparing the different re-scanning techniques [10] and their effectiveness depending on parameters such as: the number of fields, number of rescans, motion amplitude etc. [11]. One of the main concerns is the increase of the total treatment time, which depends both on the type of the re-scanning techniques used and the features of the accelerator and the dose delivery system.

In 2009 a "sparse" technique, in which not all planned spots are visited the same number of times by the beam spot, was introduced by Amaldi et al. [5] and applied to a simple case, a 1-liter water sphere. In the present paper this procedure is called *sparse proportional re-scanning* or *sparse proportional re-painting* since "re-painting" and "re-scanning" are used as synonyms. The technique is applied to a large set of clinical cases and its advantages are quantified by computing a "reduction factor", which measures the reduction of the time needed to treat a tumour when using sparse re-scanning instead of visiting all planned spots at every re-scanning.

In Sections 2.1 and 2.2, the conventional re-scanning techniques are described and compared with sparse proportional re-scanning. In Section 2.3, this technique is discussed in detail on a real tumour case. In Section 3 the results obtained from proton beam treatment plans for 15 adult and 14 paediatric tumours (54 fields) are summarized. Discussion and conclusions are presented in Sections 4 and 5 respectively.

2. Materials and methods

In order to distribute the prescribed dose to the target volume, the TPS defines, for a chosen field of irradiation:

1. the optimal number S of spots that are placed, in L Equal-Energy Layers and, in each layer, on a transverse rectangular spot grid;
2. the number of particles, or Monitor Units, computed for each one of the S planned spots, here called "weights" with symbols P_i $(1 \leq i \leq S)$.

As already mentioned, re-scanning techniques are particularly important in the case of moving targets. Indeed the interference of the motion of the particle beam and the target (interplay effects) can lead to local over and under-dosages to the target volume [12]. In order to reduce the risk of "hot" and "cold" sub-volumes of the target, three approaches have been proposed [13]:

a. the beam is switched on only when the planned spot is within a predefined spatial window, a technique that is called (respiratory) "gating" [14,15];
b. the local over-dosages and under-dosages and the spatial errors are averaged out by re-scanning [16,17];
c. the tumour is continuously followed by using a 4-dimensional feedback system. This technique is often called tumour "tracking" [18,19].

In our opinion further research could demonstrate that the combination of strategies b. and c. could drive to the best results for hadron therapy treatments. Currently the respiratory gating technique and rescanning seem to be the most clinically promising [20].

2.1. Determination of the spot multiplicities M_i

Having computed with the TPS the weight P_i (usually measured in number of particles), to be delivered by the beam spot to the i-th planned spot, and chosen the number N of re-scannings, the multiplicity M_i of the visits to the *i-th* spot (with $0 \leq M_i \leq N$) has to be defined.

To choose M_i two strategies have been proposed at Paul Scherrer Institute (PSI) with simulations [11,16] as well as experimentally [9,21]:

1. ***scaled re-scanning***: for all planned spots the numbers of visit is $M_i = N$, as indicated in Fig. 2a;
2. ***iso-layered (proportional) re-scanning***: in each layer only the highest weighted spot is visited N times, while the number of visits M_i to all the other spots are scaled down (almost) proportionally to the weight of each spot by using a "weight quantum" W. The "weight quantum" is obtained by dividing the maximum weight in the layer P_{max} by N. This quantum $W = P_{max}/N$, is used for computing the multiplicity M_i of all the spots with a compensation for the remaining weight, as shown in Fig. 2b.

In the example of Fig. 2b, the multiplicities M_i vary between 2 and $N = 12$.

2.2. Procedures for re-scanning the tumour target during a treatment

Once the multiplicities M_i of the S planned spots have been fixed, there are still many ways to deliver the dose to the target volume. They differ in two aspects: the order in which the planned spots are visited by the beam spot and the weights given when visiting, in the chosen order, M_i times the *i-th* planned spot.

As far as the order is concerned there are essentially three possibilities:

1. ***repeated delivery***, in which the whole dose, corresponding to the weight P_i is delivered to each spot in M_i visits before passing to the next spot;

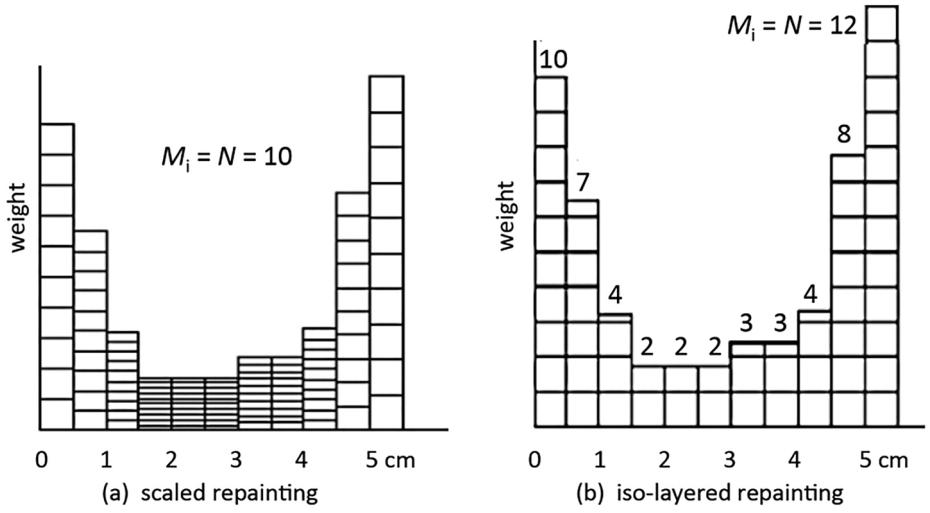

Fig. 2. The figure (adapted from [16]) refers to the transverse cut of an energy layer which contains the spot of highest weight; two procedures are compared: scaled re-scanning (for N = 10) and *iso*-layered re-scanning (for N = 12).

2. ***layered delivery***, in which each layer of the target is scanned M_{max} times before proceeding to the next layer, where M_{max} is the maximum multiplicity in the layer;
3. ***volumetric delivery***, in which the whole target is scanned fully once before repeating the same operation N-1 times;

The choice between these delivery procedures, which is strongly related to the type of accelerator and beam transport system installed in the therapy facility, is discussed in Section 4.2.

As far as the weights to be used for treatment are concerned, it has to be stressed that, even if, for computing the multiplicities M_i, one of the methods of Fig. 2 has been applied, it is often better to use a different sharing of the weights for the N-fold re-scanning of the target.

In a *first strategy*, the most obvious one, the subdivision of the weights used for the TPS computations is also used for depositing the dose in the planned spots, so that during the delivery (repeated, layered, volumetric) the weight distributions are the ones shown in Fig. 2a for a scaled delivery and to the one of Fig. 2b for a *iso*-layered proportional delivery. In this case for some planned spot one weight is smaller than the others.

In a *second strategy*, which can be called "equal deliveries procedure", each total weight P_j is divided in M_i equal deliveries so that, as shown in Table 1, the weight of the beam spot visiting for the j-th time the i-th spot is given by:

$$P_{ij} = \frac{P_i}{M_i} \tag{1}$$

2.3. Sparse proportional re-scanning and its "reduction factor"

The innumerable possible dose delivery procedures are not further discussed in this paper, which is centred on the results of the Treatment Planning System. In particular, it aims at quantifying the reduction of the *total number of planned spots* when a third procedure to compute the multiplicities M_i, is used. Here it is called "sparse proportional re-scanning", which adds to the two procedures discussed in Section 2.1. In summary:

1. ***scaled re-scanning***: for all the S planned spots the numbers of visit is $M_i = N$;
2. ***iso-layered (proportional) re-scanning***: in *each* layer the number of visits M_i are scaled (almost) proportionally to the weight P_i;
3. ***sparse (proportional) re-scanning***: in the *whole* target the number of visits M_i are scaled (almost) proportionally to the weight P_i;

In the third method the total volume is considered, and not a single layer as in the second one, and the *same* weight quantum W is used for all the S spots by applying the following algorithm:

i. the range between 0 and P_{max} – which is the number of particles corresponding to the planned spot with the maximum weight in the whole target - is divided by N to obtain the "weight quantum" W as:

$$W = \frac{P_{max}}{N} \tag{2}$$

ii. the weight of each spot Pi of the whole target is compared with the N quantities $W, 2W, 3W \ldots NW$; if P_i is in the interval between $(q-1)$ W and qW [with $1 \le q \le N$] then $M_i = q$.

The first proposal of sparse proportional re-scanning is found in [5] and concerns a 1-litre sphere re-scanned $N = 12$ times. Fig. 3a, taken from this paper, represents the total number of protons in each planned spot, belonging to the central longitudinal slice of a spherical 1-litre water target. The centre of this 62 mm radius sphere is placed in a water phantom at a depth of 200 mm and the proton beam has a width FWHM = 14 mm (σ = 5.9 mm) so that, with grid steps equal to 75% of the FWHM (i.e. to 10.5 mm), the total number of spots is 2300, corresponding to a maximum of 13 spots in the three orthogonal directions.

Fig. 3b, which represents the number of visits for one of the 13 longitudinal slices, is *similar* Fig. 3a because the number of visits is chosen to be (almost) *proportional* to the number of protons by following the steps i and ii discussed above.

In this example the number of planned spots is 2300. With 12-fold scaled re-scanning, the total number $V_{12\text{-}scaled}$ of visits is

Table 1
Fractions of the total weight P_i delivered in a five-fold re-scanning (N = 5) to a planned spot with multiplicities in the range $1 \le M_j \le 5$.

Interval of P_{ij}/P_i	M_i	P_{ij}/P_i				
		j = 1	j = 2	j = 3	j = 4	j = 5
0.00–0.20	1	1.00				
0.20–0.40	2	0.50	0.50			
0.40–0.60	3	0.33	0.33	0.34		
0.60–0.80	4	0.25	0.25	0.25	0.25	
0.80–1.00	5	0.20	0.20	0.20	0.20	0.20

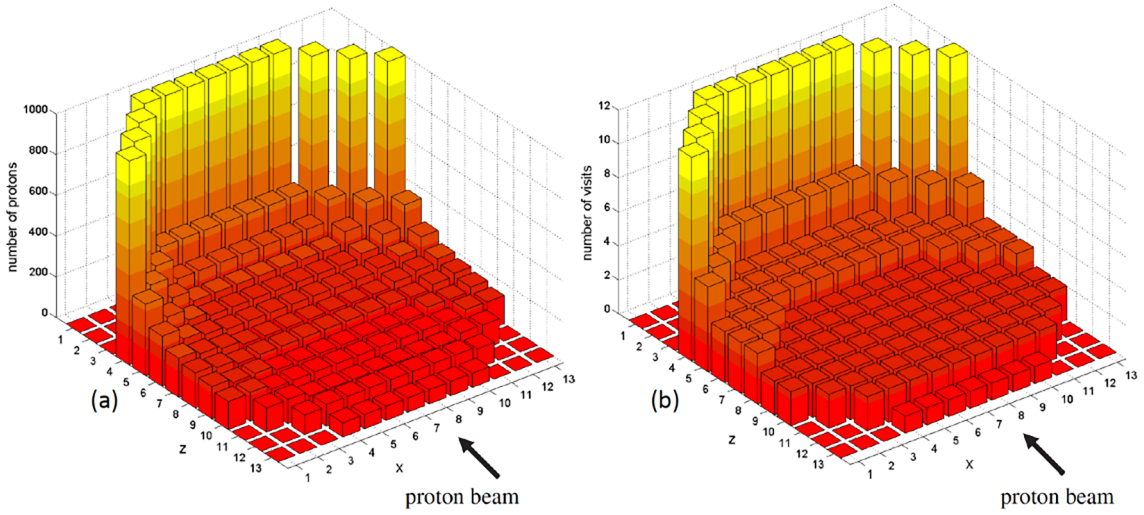

Fig. 3. (a) Distribution of the number of protons P_i for the central longitudinal section of the 1-liter water sphere. (b) Number of visits M_i to the planned spots of figure (a) for a 12-fold re-scanning [5].

$V_{12\text{-}scaled} = NS = 12 \times 2300 = 27\ 600$. When 12-fold sparse proportional re-scanning is applied, the Treatment Planning System produces 13 images similar to Fig. 3b by requiring that the sphere is uniformly irradiated. By summing the number of visits in these 13 figures one obtains the total number $V_{12\text{-}sparse} = 8100$.

The gain in passing from a *N*-fold scaled proportional re-scanning to a *N*-fold sparse proportional re-scanning is quantified by the "reduction factor" defined as:

$$reduction\ \ factor\ \ RF\ \ (N) = \frac{V_{N-scaled}}{V_{N-sparse}} = \frac{NS}{V_{N-sparse}} \tag{3}$$

For the example of the water sphere the reduction factor is:

$$reduction\ \ factor\ \ RF\ \ (12) = \frac{V_{12-scaled}}{V_{12-sparse}} = 12 \times \frac{2300}{8100} = 3.4 \tag{4}$$

The reduction factor RF depends, in principle, on not only the number of re-scannings *N*, but also on the shape of the tumour, the number of layers *L* and the dimensionality of the spot grid into which the tumour target is subdivided. In the next section, the reduction factor is computed for 29 clinical cases (54 fields) to check whether the same value 3.4 is obtained for many different shapes and volumes of the tumour target. It will be shown that the reduction factor is a function of *N* and nothing else.

As discussed in Section 2.3, having fixed the multiplicity M_i of the planned spots there are infinitely many possibilities to deposit the dose during the treatment. Fig. 4 describes an equal deliveries procedure, which is characterized by Eq. (1). In this delivering procedure all the planned spots are visited with approximately the *same* dose rate; when the maximum dose rate is used this minimizes the treatment time.

Note that the planned spots, which are not on the distal border of the target, "see" protons a number of times that is always larger than M_i because they are traversed by the beam visiting downstream spots.

To help the reader Table 2 lists the definitions of the quantities used in this paper.

3. Results

3.1. Detailed discussion of one clinical case

To evaluate the reduction factors for clinically relevant cases, treatment plans were computed for 15 adult patient cases (27 proton fields) and 14 paediatric patients (27 proton fields) with the *Eclipse™ for Proton* treatment planning system from Varian Medical Systems, which uses a proton optimization algorithm to produce a conformal dose distribution, usually delivered in a single scanning [22].

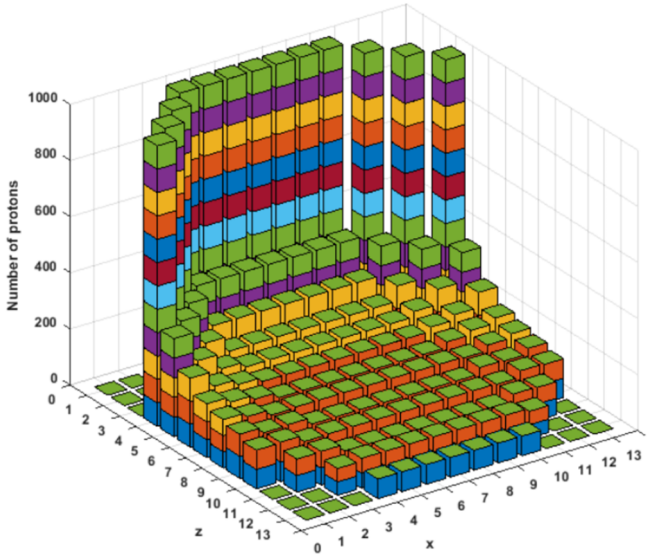

Fig. 4. The doses deposited in 12 successive visits to the planned spots of the longitudinal slice of Fig. 3 are shown in different colours for an equal deliveries procedure.

As a first step, the treatment plan of each clinical case was optimised for a single scanning treatment following the clinical protocols for the dose prescription to the target volume and dose constraints to the Organs At Risk (OARs). Then the sparse proportional re-scanning procedure was applied to the dose distribution produced by Eclipse™.

To introduce the argument, in this Section the single scanning treatment plan for one of the adult patients with a lung tumour (A01) is described and the sparse procedure applied.

The margin of the target volumes – Clinical Target Volume (CTV) and Planning Target Volume (PTV) – and the organs at risk (OARs) for adult patient A01 are displayed in Fig. 5a. The volumes of the CTV and PTV are 350 cm^3 and 510 cm^3 respectively and the prescribed dose is 50 Gy in 25 fractions. According to the prescription, the dose distribution of the patient A01 is shown in Fig. 5b.

For this patient, a single irradiation field was sufficient to deliver the prescribed dose. The properties of the field are summarized in Table 3, where the *spot spacing* (Δ) indicates the transverse distance between the centres of two contiguous planned spots.

Table 2
Definitions of the quantities used in this paper.

S	Number of planned spots covering the tumour target according to the TPS
L	Number of layers
Δ	Spot spacing in the transverse spot grid
P_i	Weight for the i-th planned spot, measured in number of particles
P_{max}	Weight (or nb. of particles) for the spot with the maximum weight
N	Nb. of re-scannings = number of visits by the beam spot to the planned spots
M_i	Multiplicity of the i-th spot = number of visits to the i-th planned spot
W	Weight quantum $W = P_{max}/N$ used for the multiplicities M_i – Eq. (2)
P_{ij}	Weight (or number of protons) of the j-th visit to the i-th planned spot
$V_{N\text{-scaled}}$	Number of visits in scaled re-scanning with N re-scannings = NS
$V_{N\text{-sparse}}$	Number of visits in sparse proportional re-scanning with N re-scannings
$RF(N)$	Reduction factor as defined by Eq. (3) = $V_{N\text{-scaled}}/V_{N\text{-sparse}} = NS/V_{N\text{-sparse}}$
$f(N)$	Normalized reduction factor = $RF(N)/RF(12)$
S_k	Number of spots visited k times by the beam spot
t_{scan}	Average time required to change the currents of the Scanning Magnets
T_{scan}	Total scanning time for sparse spot re-scanning = $NS\ t_{scan}/RF(N)$
t_{change}	Average switching time from one energy layer to the next
T_{change}	Total energy switching time in the longitudinal direction ($\leq N\,L\,t_{change}$)
T_{irr}	Total irradiation time = $T_{scan} + T_{change}$, as given by Eq. (10)

The sparse proportional re-scanning technique explained in Section 2.3 was applied to the optimized treatment. This requires identifying the planned spot that in the entire target volume has the highest weight, defining the weight quantum W and then using to determine the number of visits.

For a number of re-scanning $N = 12$, the distribution of the number of visits for a central longitudinal slice is shown in Fig. 6. Only the distal high-weighted spots receive 12 visits, while the number of visits decrease rapidly for the close to the skin low-weighted planned spots.

For the adult patient A01, Table 4 shows the number of spots that receive one visit, two visits, three visits, and so on. In single scanning – column (2) – all the tumour spots (S = 2303) are visited once so that the total number of visits is $V_1 = 2303$. For scaled re-scanning – column (3) – all the spots are visited 12 times for a total number of visits $V_{12\text{-}scaled} = 27.636$. For sparse proportional re-scanning column (4) lists the number of spots that are visited once, twice, three times, etc. By summing the data of column (4) one obtains $V_{12\text{-}sparse} = 6730$, which corresponds to a reduction factor

$$reduction\ \ factor RF(12) = \frac{V_{12-scaled}}{V_{12-sparse}} = \frac{27636}{6730} = 4.1 \quad (5)$$

In Table 4, by aggregating the numbers of column (4), the figures of columns (5) and (6) have been obtained so to compute the reduction factors for $N = 6$ an $N = 3$ shown in the last row. To obtain a result applicable to all targets in Fig. 7 these figures have been normalized to $RF(12)$ by computing the fractions:

$$f(12) = RF(12)/RF(12) = 1.0,\ f(6) = RF(6)/RF(12) = 3.40/4.11 = 0.83,$$

$$f(3) = RF(3)/RF(12) = 2.41/4.11 = 0.59,\ f(1) = 1/RF(12) = 0.24.$$

Since the ratios f(N) depend only on the longitudinal distribution of the energy deposited in soft tissues and not on the shape and volume of the tumour target, the dashed curve of Fig. 7 can be used for all tumours. For instance, for 5 re-scannings – a choice proven to be an

Table 3
Parameters of the field used in the treatment plan.

		Field 1
Number of layers	L	24
Spot transverse spacing (mm)	Δ	6
Number of spots	S	2303
Max Energy (MeV)		182.2
Min Energy (MeV		87.3

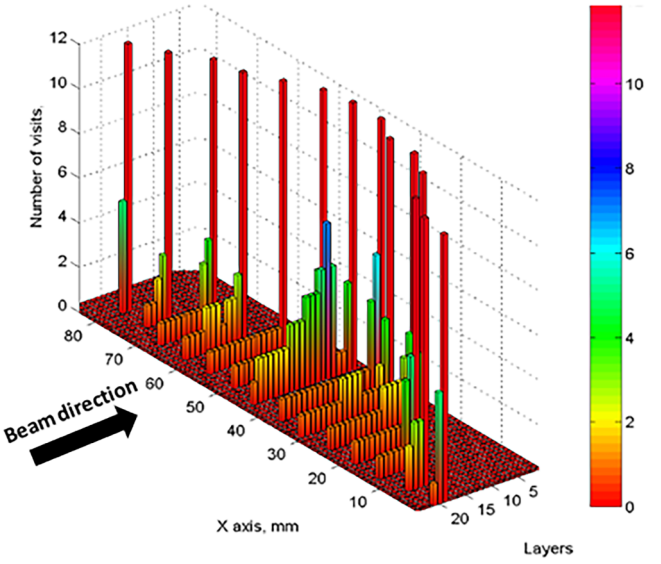

Fig. 6. Distribution of the number of visits for a central longitudinal slice through the tumour as a function of depth.

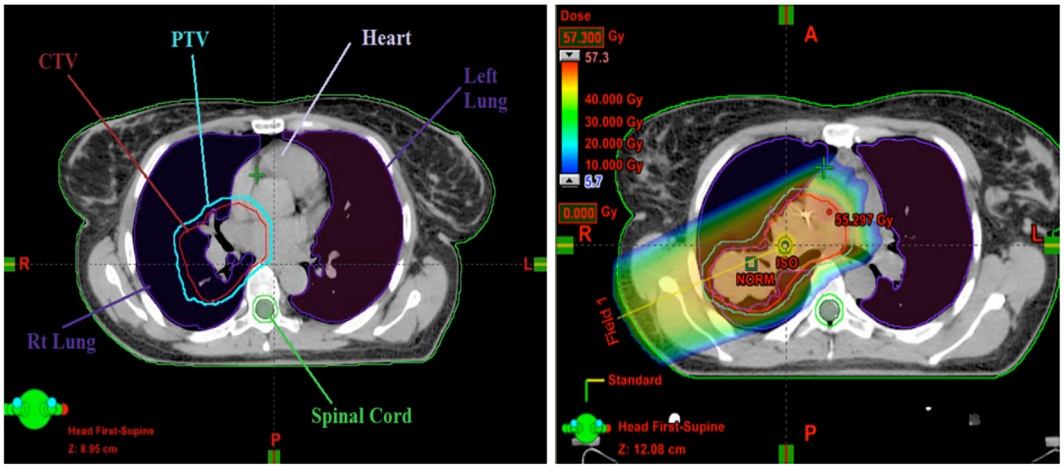

(a) Target volume and OARs (b) Dose distribution

Fig. 5. Target structures and optimized dose distribution for the adult patient A01.

Table 4
Number of spots S_k that receive 1 visit, 2 visits, 3 visits… k visits and the total number of visits, V = Σ S_k × k, for five different re-scanning strategies.

(1) Nb of visits k	(2) Single scanning $S_k \times k$	(3) 12-fold scaled re-scanning $S_k \times k$	(4) Sparse 12-fold re-scanning ($N = 12$) $S_k \times k$	(5) Sparse 6-fold re-scanning ($N = 6$) $S_k \times k$	(6) Sparse 3-fold re-scanning ($N = 3$) $S_k \times k$
1	2303 × 1	0	1124 × 1	1604 × 1	1984 × 1
2	0	0	480 × 2		
3	0	0	223 × 3	380 × 2	
4	0	0	157 × 4		
5	0	0	55 × 5	66 × 3	70 × 2
6	0	0	11 × 6		
7	0	0	4 × 7	4 × 4	
8	0	0	0 × 8		
9	0	0	2 × 9	3 × 5	249 × 3
10	0	0	1x 10		
11	0	0	0 × 11	246 × 6	
12	0	2303 × 12	246 × 12		
	V_1 = 2303	$V_{12\text{-scaled}}$ = 27.636	$V_{12\text{-sparse}}$ = 6730	$V_{6\text{-sparse}}$ = 4069	$V_{3\text{-sparse}}$ = 2871
	Reduction factor		**4.11**	**3.40**	**2.41**
	$\boldsymbol{RF(N) = V_{12\text{-scaled}}/V_{N\text{-sparse}}}$				

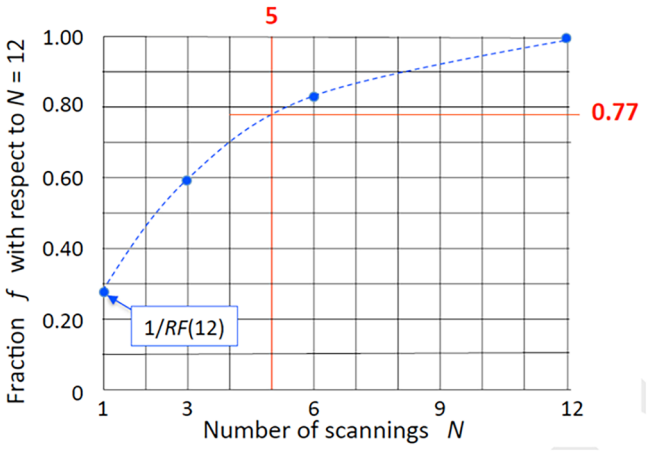

Fig. 7. The reduction factors RF(N) are obtained by multiplying f(N) by RF(12).

optimal by [23]– one can use the formula

$$RF(5) = f(5)RF(12) = 0.77RF(12). \quad (6)$$

To conclude the detailed study of case A01, in Table 5 each element x_{ij} indicates how many spots belonging to the layer i are visited during the j-th scanning, where i is the row index and j is the column index. The last row "Tot" gives the number of spots that are visited during the j-th scanning; the sum is $V_{12\text{-sparse}} = 6730$.

Finally in Table 6 a comparison between single scanning and sparse re-scanning is presented for $N = 12$ and $N = 5$.

3.2. Summary of the results obtained on 29 clinical cases

As anticipated, the same study performed on patient A01 was repeated for other 14 adult patients (27 proton fields) and 14 paediatric patients (27 proton fields). The results are summarized in Tables 7 and 8.

The *reduction factors RF*(12) – indicated as *RF* in Tables 7 and 8– are in the range 2.6–4.5. The distributions for adult and children patients, plotted in Fig. 8, are superimposable and have the same r.m.s. value of 0.40.

Averaging on the 27 + 27 = 54 fields of Tables 7 and 8, the 12-fold reduction factor is given by:

$$RF(12) = 3.6 \pm 0.4, \quad (7)$$

which is equal to the reduction factor $RF(12) = 3.4$ of Eq. (4), obtained for a 1-litre sphere subdivided in 13 layers.

It has to be noted that the case-to-case fluctuations quoted in Eq. (7) cover the slightly positive correlation, appearing in the data of Table 7 and Table 8, for which *RF*(12) is somewhat larger for bigger targets.

4. Discussion

4.1. A unique value of the reduction factor for all tumours

The results presented in Section 3.2 demonstrate that, within about ± 10%, the reduction factor *RF*(N) does not depend on the shape of the tumour target, the spacing Δ of the spot grid, the number of layers - which varies in the wide range that goes from 13 (patient P06) to 24 (patient A01- and its volume - which in the 29 studied cases varies between 13 cm^3 (patient P06) and 870 cm^3 (patient A06).

In conclusion Fig. 7 can be used to scale the reduction factor and the summary graph of Fig. 9 is valid for all tumours.

From Fig. 9 one can read that in the optimal five-fold re-scanning procedure the reduction factor is

$$RF(5) = 2.8 \pm 0.3 \quad (8)$$

It has been shown that, for a given target shape, the reduction factor *RF*(N) does not depend on the target thickness D, the number of layers L and the spot grid spacing Δ. However, it certainly depends on the depth dose distribution. In particular, it has to be a function of the ratio D/W_B where W_B is the FWHM width of the Bragg peak.

Although the width W_B of a carbon Bragg is about three times smaller than for proton, in clinical carbon treatments, ridge filters are used to enlarge the width of the Bragg peak. In this way protons and carbon ions have comparable Bragg peak width so the computation of the *RF*(N) leads to the same results.

Eqs. (7) and (8) and Fig. 9 can thus be used also for the treatments with carbon ions. For thicker targets the slight positive correlation noted at the end of Section 3.2, covered by the case-to case ± 10% fluctuations, guarantees that the curves of Fig. 9 represent, within the quoted uncertainty, the carbon ions reduction factors.

4.2. Effects of the reduction factor on the irradiation time

In the sparse proportional N-fold re-scanning of a tumour target – which is covered by S planned spots – the number of visits $V_{N\text{-sparse}}$ is obtained dividing the product NS (which is the number of visits in a scaled re-scanning of the same target) by the value *RF*(N) obtained from Fig. 9:

$$V_{N-sparse} = \frac{NS}{RF(N)} \quad (9)$$

This result of Eq. (9) is applicable to any irradiation procedures (repeated, layered, volumetric…) and also when tumour tracking is

Table 5
Distribution of the number of visits for N = 12 re-scannings. The rows represent the layers, and the columns indicate the ordinal number of the re-scannings from 1 to 12. Each layer corresponds to a different beam energy.

Layer index	Energy (MeV)	Ordinal number of the 12 re-scannings											
		1st	2nd	3rd	4th	5th	6th	7th	8th	9th	10th	11th	12th
1	182.19	1	1	1	1	1	1	1	1	1	1	1	1
2	178.97	6	6	6	6	5	5	5	5	5	5	5	5
3	175.70	15	15	15	13	9	9	9	9	9	9	9	9
4	172.39	26	26	24	18	13	12	11	11	11	11	11	11
5	169.02	34	30	25	19	10	9	8	8	8	8	8	8
6	165.57	46	35	24	18	13	12	12	12	12	12	12	12
7	162.04	60	45	31	25	16	14	14	14	14	14	14	14
8	158.40	69	52	32	20	14	10	10	9	9	9	9	9
9	154.64	90	62	39	28	23	22	22	22	22	22	22	22
10	150.74	121	81	57	43	33	31	31	31	31	31	31	31
11	146.69	133	88	66	46	23	19	19	19	19	19	19	19
12	142.46	137	93	61	31	20	14	13	13	13	12	12	12
13	138.18	141	89	47	21	15	11	9	7	7	7	7	7
14	133.94	145	75	33	20	15	10	9	9	9	9	9	9
15	129.71	160	82	39	28	20	20	20	20	20	20	20	20
16	125.45	158	73	35	22	13	10	10	10	10	10	10	10
17	121.16	164	76	37	27	15	12	12	12	12	12	12	12
18	116.79	161	64	36	26	19	12	11	11	11	11	11	11
19	112.32	165	59	35	26	20	13	10	10	10	10	10	10
20	107.73	158	56	27	19	10	8	7	7	7	7	7	7
21	102.97	147	43	19	13	8	7	7	7	7	7	7	7
22	98.00	104	26	10	6	4	3	3	2	2	1	0	0
23	92.78	52	2	0	0	0	0	0	0	0	0	0	0
24	87.25	10	0	0	0	0	0	0	0	0	0	0	0
	Tot	**2303**	**1179**	**699**	**476**	**319**	**264**	**253**	**249**	**249**	**247**	**246**	**246**

used to follow a moving tumour [24]. Indeed the calculation of the reduction factor does not depend on the movements of the target.

Sparse proportional re-scanning reduces the treatment time with respect to the other methods of determining the multiplicities M_i of the S planned spots. This advantage is at present very important since the shortening of the irradiation is a topical subject in radiation therapy.

To determine the conditions in which sparse volumetric Spot Scanning procedures are advantageous, one has to take into account that the irradiation time T_{irr} depends on many parameters: the number of planned spots S of that field, the number L of layers, the number N of re-scannings, the *average* time t_{scan} required to both change the currents of the two orthogonal scanning magnets, displacing the beam spot from one planned spot to the next, and to deliver the dose, and the time (t_{change}) required to change layer (i.e. beam energy):

$$T_{irr} = T_{scan} + T_{change} \cong NSt_{scan}/RF(N) + NLt_{change} \,(\textit{sparse volumetric delivery}). \tag{10}$$

Note that T_{change} can be smaller than $NL\,t_{change}$ if, in some of the N re-scannings, one or more layers have not to be visited.

In a well-designed treatment the second term of Eq. (10) has to be definitely smaller than the first one:

$$t_{change} << (S/L)\; t_{scan}/RF(N) \cong 500 - 1000 \text{ ms}, \tag{11}$$

with the typical values $L = 22$, $S = 3000$ – valid for a 0.1–0.5 L targets (Table 6), $RF(5) = 2.8$ from. Eq. (8) and a displacement and delivery average time t_{scan} = 10–20 ms. For a conventional scanning with $N = 1$, in which all the S planned spots are visited once, this choice of t_{scan} corresponds to a S t_{scan} = 30–60 s.

Note that in a sparse volumetric delivery:

1. to shorten t_{scan}, the transverse movements of the beam spot have to be optimized in each layer as in a travelling salesman problem,
2. after this procedure the *average* displacement time of the spot gives a small contribution to t_{scan} because it is not larger than 3 ms (out of f t_{scan} = 10–20 ms) for a spot transverse speed of 10 m/s and a 30 mm *average* displacement, which is 1/3 of the transverse dimensions of the largest targets.

Of course, in a conventional procedure – in which all the S spots are visited in sequence – the average displacement time, needed to move the spot by one step, is equal to about 1 ms because the movements are typically about 10 mm. However, the overall average displacement and delivery time is shorter by (3–1 ms)/(10–20 ms) ≅10–20% only with respect to a sparse volumetric procedure.

Inequality (11) says that, to effectively apply the sparse volumetric proportional delivery procedure introduced in this paper, the time for changing layer has to be

$$t_{change} \leqslant 100 - 200 \text{ ms } (\textit{sparse volumetric delivery}). \tag{12}$$

If this condition is not satisfied, sparse layered Spot Scanning

Table 6
Comparison between single scanning and sparse re-scanning for adult patient A01 with a 510 cm^3 target volume.

		Single scanning	Sparse 12-fold re-scanning	Sparse 5-fold re-scanning
Number of re-scannings	N	1	12	5
Number of energy layers	L	24	24	24
"Visited" energy layers	L_{tot}	24	265	120
Number of planned spots	S	2303	2303	2303
Reduction factor from Eqs. (3) and (4)	RF	–	4.1	3.2
Number of visits	V_N	2303	2303 × 12/4.1 = 6740	2303 × 5/3.2 = 3600
Max nb. of protons in a visit	P_{max}	$7.1 \cdot 10^8$	$5.9 \cdot 10^7$	$1.4 \cdot 10^8$

Table 7
Summary of 12-fold sparse proportional re-scanning for 15 adult tumours (27 proton fields). For patients with more than one row, the optimized plan contained multiple fields.

Vol. cm^3	L/Δ mm	S	$V_{12\text{-sparse}}$	RF	Vol. cm^3	L/Δ mm	S	$V_{12\text{-sparse}}$	RF
Lung					**A08**-490	23/6	2 155	7 463	**3.5**
A01-510	24/6	2 303	6 730	**4.1**		21/6	2 359	7 567	**3.7**
A02-209	20/2	12 621	48 485	**3.1**	**Brain**				
	19/2	14 071	45 744	**3.7**	**A09**-104	21/6	1 055	3 443	**3.7**
	18/2	11 515	40 073	**3.4**	**A10**-56	17/2	6 055	23 996	**3.0**
A03-803	22/6	2 772	9 990	**3.3**	**Liver**				
	22/6	2 768	10 189	**3.2**	**A11**-235	17/6	1 719	5 393	**3.8**
	20/6	3 166	10 085	**3.8**	**A12**-473	16/6	2 721	9 207	**3.5**
A04-406	21/6	2 167	8 301	**3.1**		18/6	2 711	9 929	**3.3**
	21/6	2 706	7 389	**3.5**	**Lymphoma**				
	24/6	1 821	6 830	**3.2**	**A13**-225	17/6	1 585	5 041	**3.8**
A05-430	20/6	2 535	7 305	**4.2**		18/6	1 751	5 584	**3.8**
	21/6	2 694	8 002	**4.0**	**Prostate**				
A06-870	23/6	4 147	11 472	**4.3**	**A14**- 38	10/6	401	1 837	**2.6**
	22/6	3 911	11 397	**4.1**	**A15**-120	12/6	755	3 045	**3.0**
A07-450	23/2	25 949	74 067	**4.2**		12/6	764	3038	**3.0**
					Average				**3.5**

delivery has to be adopted since in this case the factor multiplying Eq. (10) is L instead than NL [23].

As discussed in Section 1, the minimal times in (synchro)cyclotrons and synchrotrons can respect Eq. (12) while for hadron linacs t_{change} is 3–5 ms, more than 10 times smaller than the quoted limit. Linacs are much faster than cyclotrons and synchrotrons but the advantages in irradiation times are not large, as demonstrated by comparing the 5-fold volumetric irradiation times for the above defined typical target, introducing in Eq. (11) $t_{scan} = 10$ ms and the two choices $t_{change} = 5$ ms (linacs) and $t_{change} = 150$ ms (cyclotrons and synchrotrons). The two treatments last 53.7 s and 70.2 s respectively, which differ by 30%.

From these figures it would seem that volumetric delivery procedures can be used with all therapy systems. However, the fixed and rotating transport lines, guiding the beam from the accelerator to the patient, most often are slow and do not satisfy Eq. (12). This is the reason for which at present major commercial companies using proton (synchro)cyclotrons choose, for their "slow" gantries, layered delivery procedures with $t_{change} \geq 500$ ms.

Three methods have been proposed to bypass this limitation.

The first one is centred on the development of large momentum acceptance transport lines, so that the magnet currents are kept fixed while, during the treatment of a tumour, the energy of the beam changes by ± 10–15%. At present large momentum acceptance gantries are under development by many groups, in particular at BNL, LBL [25,26] and PSI [27].

Secondly, the power supplies of the magnets, forming the fixed and rotating lines, can be "fast" so that energy changes of the beam can be followed in times that are of the order of 5 ms, definitely shorter than the 100–200 ms of Eq. (12). This is the method proposed by TERA for hadron linacs [28].

Recently a third approach has been proposed: the currents of all the bending magnets and quadrupoles of the transport line are varied synchronously so to follow the continuously variable energy of the hadron beam and perform what has been called a "Oblique Raster Scanning" of the tumour target [29].

5. Conclusions

Sparse proportional Spot Scanning is a N-fold re-scanning dose delivery procedure in which only a fraction of the planned spots is visited by the beam spot N times. This method reduces both the errors in the dose distributions and the irradiation times, in particular in the case of volumetric re-scanning, which has been demonstrated in the literature to be the best delivery procedure in case of moving organs.

Table 8
Summary of 12-fold sparse proportional re-scanning for 14 paediatric tumours (27 proton fields). For patients with more than one row, the optimized plan contained multiple fields.

Vol. cm^3	L/Δ mm	S	$V_{12\text{-sparse}}$	RF	Vol. cm^3	L/Δ mm	S	$V_{12\text{-sparse}}$	RF
Posterior fossa					**Temporal lobe**				
P01-25	17/2	3 738	13 839	**3.2**	**P08**-155	17/6	1 267	4 114	**3.7**
	15/2	3 827	14 857	**3.1**	**Nasopharynx**				
	16/2	3 560	13 018	**3.3**	**P09**-100	19/2	10 557	33 496	**3.8**
P02-19	13/2	3 510	14 863	**2.8**		20/2	11 021	33 340	**4.0**
	15/2	3 506	12 997	**3.2**	**Brain**				
	15/2	3 267	11 632	**3.4**	**P10**-108	16/6	934	2 719	**4.1**
P03-33	15/2	4 680	16 033	**3.5**		14/6	618	2 084	**3.6**
P04-67	18/2	8 751	23 719	**4.4**		18/6	989	2 949	**4.0**
Hypothalamus					**Cranio-spinal**				
P05-235	20/2	19 113	51 027	**4.5**	**P11**-41	19/2	5 963	18 573	**3.9**
	20/2	18 030	49 730	**4.3**	**P12**-56	17/6	720	2 323	**3.7**
P06-13	13/2	2 582	10 148	**3.1**	**P13**-40	15/2	4 518	15 907	**3.4**
	13/2	2 542	10 317	**3.0**		16/2	5 468	17 171	**3.8**
Ependynoma		15/2	4 889	16 913	**3.5**				
P07-70	19/2	8 083	24 824	**3.9**	**Mediastinum**				
	17/2	7 350	24 263	**3.6**	**P14**-205	17/2	2 175	36 583	**4.0**
	18/2	8 896	27 398	**3.9**					
					Average				**3.7**

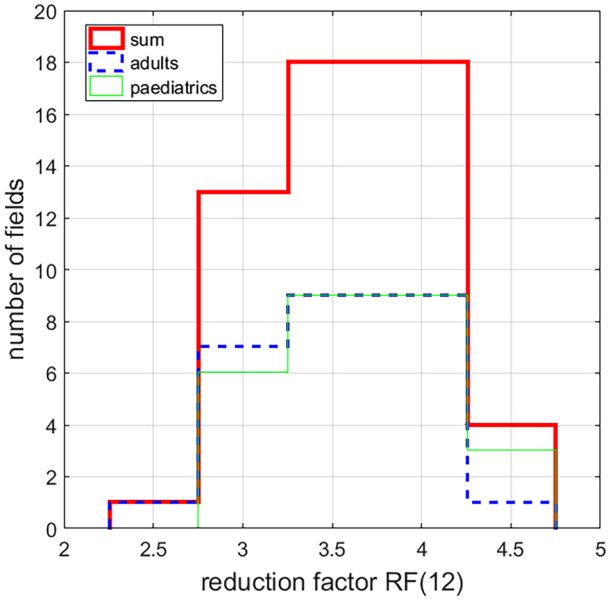

Fig. 8. Histograms of RF(12) for the 54 fields of Tables 7 and 8.

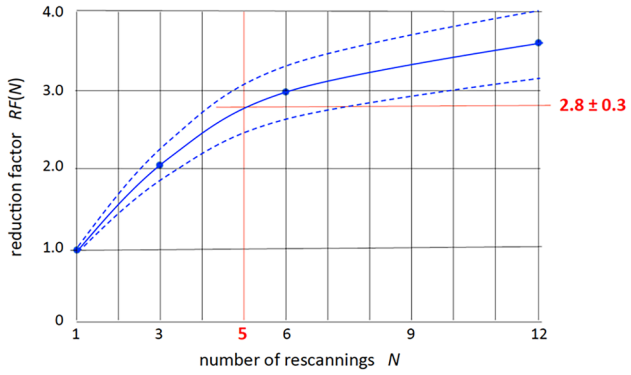

Fig. 9. The reduction factor RF(N) is plotted versus the number N of re-scannings.

The advantages of sparse proportional re-scanning have been quantified by introducing a parameter, the reduction factor *RF*(*N*), which has been proven with a detailed study of 54 proton treatment plans to be a function of the number of re-scannings *N* (Fig. 9) but not to depend neither on the shape and the volume of the tumour nor on the distance between the scanned layers. Fig. 9 shows that for $N = 5$ and $N = 12$ the reduction factors are 2.8 ± 0.3 and 3.6 ± 0.4 respectively. These numbers are also applicable in the case of treatments with carbon ion beams.

Acknowledgments

The authors are very grateful to Varian Medical Systems for the use of the Eclipse software and the workstation on which the 54 treatment plans have been computed.

References

[1] Haberer T, Becher W, Schardt D, Kraft G. Magnetic scanning system for heavy ion therapy. Nucl Inst Methods Phys Res A 1993. https://doi.org/10.1016/0168-9002(93)91335-K.
[2] Pedroni E, Bacher R, Blattmann H, Bohrinaer T, Coray A, Lomax A, et al. The 200-Mev proton therapy project at the Paul Scherrer Institute: conceptual design and practical realization. Med Phys 1995. https://doi.org/10.1118/1.597522.
[3] Ulmer W, Schaffner B. Foundation of an analytical proton beamlet model for inclusion in a general proton dose calculation system. Radiat Phys Chem 2011. https://doi.org/10.1016/j.radphyschem.2010.10.006.
[4] Mizushima K, Furukawa T, Iwata Y, Hara Y, Saotome N, Saraya Y, et al. Performance of the HIMAC beam control system using multiple-energy synchrotron operation. Nucl Instrum Methods Phys Res Sect B Beam Interact Mater Atoms 2017. https://doi.org/10.1016/j.nimb.2017.03.051.
[5] Amaldi U, Braccini S, Puggioni P. High frequency linacs for hadrontherapy. Rev Accel Sci Technol 2009. https://doi.org/10.1142/s179362680900020x.
[6] Lomax AJ, Böhringer T, Bolsi A, Coray D, Emert F, Goitein G, et al. Treatment planning and verification of proton therapy using spot scanning: Initial experiences. Med Phys 2004. https://doi.org/10.1118/1.1779371.
[7] Kardar L, Li Y, Li X, Li H, Cao W, Chang JY, et al. Evaluation and mitigation of the interplay effects of intensity modulated proton therapy for lung cancer in a clinical setting. Pract Radiat Oncol 2014. https://doi.org/10.1016/j.prro.2014.06.010.
[8] Albertini F, Hug EB, Lomax AJ. Is it necessary to plan with safety margins for actively scanned proton therapy? Phys Med Biol 2011. https://doi.org/10.1088/0031-9155/56/14/011.
[9] Schätti A, Zakova M, Meer D, Lomax AJ. Experimental verification of motion mitigation of discrete proton spot scanning by re-scanning. Phys Med Biol 2013. https://doi.org/10.1088/0031-9155/58/23/8555.
[10] Bernatowicz K, Lomax AJ, Knopf A. Comparative study of layered and volumetric rescanning for different scanning speeds of proton beam in liver patients. Phys Med Biol 2013. https://doi.org/10.1088/0031-9155/58/22/7905.
[11] Knopf AC, Lomax AJ. In the context of radiosurgery – pros and cons of rescanning as a solution for treating moving targets with scanned particle beams. Phys Medica 2014. https://doi.org/10.1016/j.ejmp.2014.03.010.
[12] Bert C, Grözinger SO, Rietzel E. Quantification of interplay effects of scanned particle beams and moving targets. Phys Med Biol 2008. https://doi.org/10.1088/0031-9155/53/9/003.
[13] Bert C, Durante M. Motion in radiotherapy: particle therapy. Phys Med Biol 2011. https://doi.org/10.1088/0031-9155/56/16/R01.
[14] Minohara S, Kanai T, Endo M, Noda K, Kanazawa M. Respiratory gated irradiation system for heavy-ion radiotherapy. Int J Radiat Oncol Biol Phys 2000. https://doi.org/10.1016/S0360-3016(00)00524-1.
[15] Bert C, Gemmel A, Saito N, Rietzel E. Gated irradiation with scanned particle beams. Int J Radiat Oncol Biol Phys 2009. https://doi.org/10.1016/j.ijrobp.2008.11.014.
[16] Zenklusen SM, Pedroni E, Meer D. A study on repainting strategies for treating moderately moving targets with proton pencil beam scanning at the new gantry 2 at PSI. Phys Med Biol 2010. https://doi.org/10.1088/0031-9155/55/17/014.
[17] Engwall E, Glimelius L, Hynning E. Effectiveness of different rescanning techniques for scanned proton radiotherapy in lung cancer patients. Phys Med Biol 2018. https://doi.org/10.1088/1361-6560/aabb7b.
[18] Parodi K, Saito N, Chaudhri N, Richter C, Durante M, Enghardt W, et al. 4D in-beam positron emission tomography for verification of motion-compensated ion beam therapy. Med Phys 2009. https://doi.org/10.1118/1.3196236.
[19] Zhang Y, Knopf A, Tanner C, Lomax AJ. Online image guided tumour tracking with scanned proton beams: a comprehensive simulation study. Phys Med Biol 2014. https://doi.org/10.1088/0031-9155/59/24/7793.
[20] Charlie Ma C-M, Lomax AJ. Proton and carbon ion therapy. CRC Press Taylor & Francis Group; 2013.
[21] Zhang Y, Huth I, Wegner M, Weber DC, Lomax AJ. An evaluation of rescanning technique for liver tumour treatments using a commercial PBS proton therapy system. Radiother Oncol 2016. https://doi.org/10.1016/j.radonc.2016.09.011.
[22] https://www.varian.com/oncology/products/software/treatment-planning/eclipse-proton.
[23] Knopf AC, Hong TS, Lomax A. Scanned proton radiotherapy for mobile targets – the effectiveness of re-scanning in the context of different treatment planning approaches and for different motion characteristics. Phys Med Biol 2011. https://doi.org/10.1088/0031-9155/56/22/016.
[24] Kubiak T. Particle therapy of moving targets-the strategies for tumour motion monitoring and moving targets irradiation. Br J Radiol 2016. https://doi.org/10.1259/bjr.20150275.
[25] Trbojevic D, Parker B, Keil E, Sessler AM. Carbon/proton therapy: a novel gantry design. Phys Rev Spec Top - Accel Beams 2007. https://doi.org/10.1103/PhysRevSTAB.10.053503.
[26] Brouwer L, Caspi S, Hafalia R, Hodgkinson A, Prestemon S, Robin D, et al. Design of an achromatic superconducting magnet for a proton therapy gantry. IEEE Trans Appl Supercond 2017. https://doi.org/10.1109/TASC.2016.2628305.
[27] Gerbershagen A, Meer D, Schippers JM, Seidel M. A novel beam optics concept in a particle therapy gantry utilizing the advantages of superconducting magnets. Z Med Phys 2016. https://doi.org/10.1016/j.zemedi.2016.03.006.
[28] Garonna A, Alharbi N, Amaldi U, Benedetto E, Ljubicic V, Riboni PL. Delivery and gantry concepts from TERA. Presentation at Workshop on Ideas and technologies for a next generation facility for medical research and therapy with ions, Archamps (ESI) 2018, https://indico.cern.ch/event/682210/contributions/2997883/attachments/1671379/2711300/20180620_PIMMS2workshopAG_v7_-_filt.pdf n.d.
[29] Amaldi U. Oblique raster scanning: an ion dose delivery procedure with variable energy layers. Phys Med Biol 2019;64(11):115003. https://doi.org/10.1088/1361-6560/ab0920.